REPORT

OPEN ACCESS

Photopyroelectric tweezers for versatile manipulation

Fang Wang,[1,5] Cong Liu,[1,2,5] Zhengjin Dai,[1,4,5] Weizhong Xu,[1] Xinyue Ma,[1] Yufeng Gao,[1] Xuewu Ge,[4] Wei Zheng,[1] and Xuemin Du[1,2,3,*]

*Correspondence: xm.du@siat.ac.cn

Received: June 12, 2024; Accepted: November 22, 2024; Published Online: December 12, 2024; https://doi.org/10.1016/j.xinn.2024.100742

© 2024 The Author(s). Published by Elsevier Inc. on behalf of Youth Innovation Co., Ltd. This is an open access article under the CC BY-NC-ND license (http://creativecommons.org/licenses/by-nc-nd/4.0/).

GRAPHICAL ABSTRACT

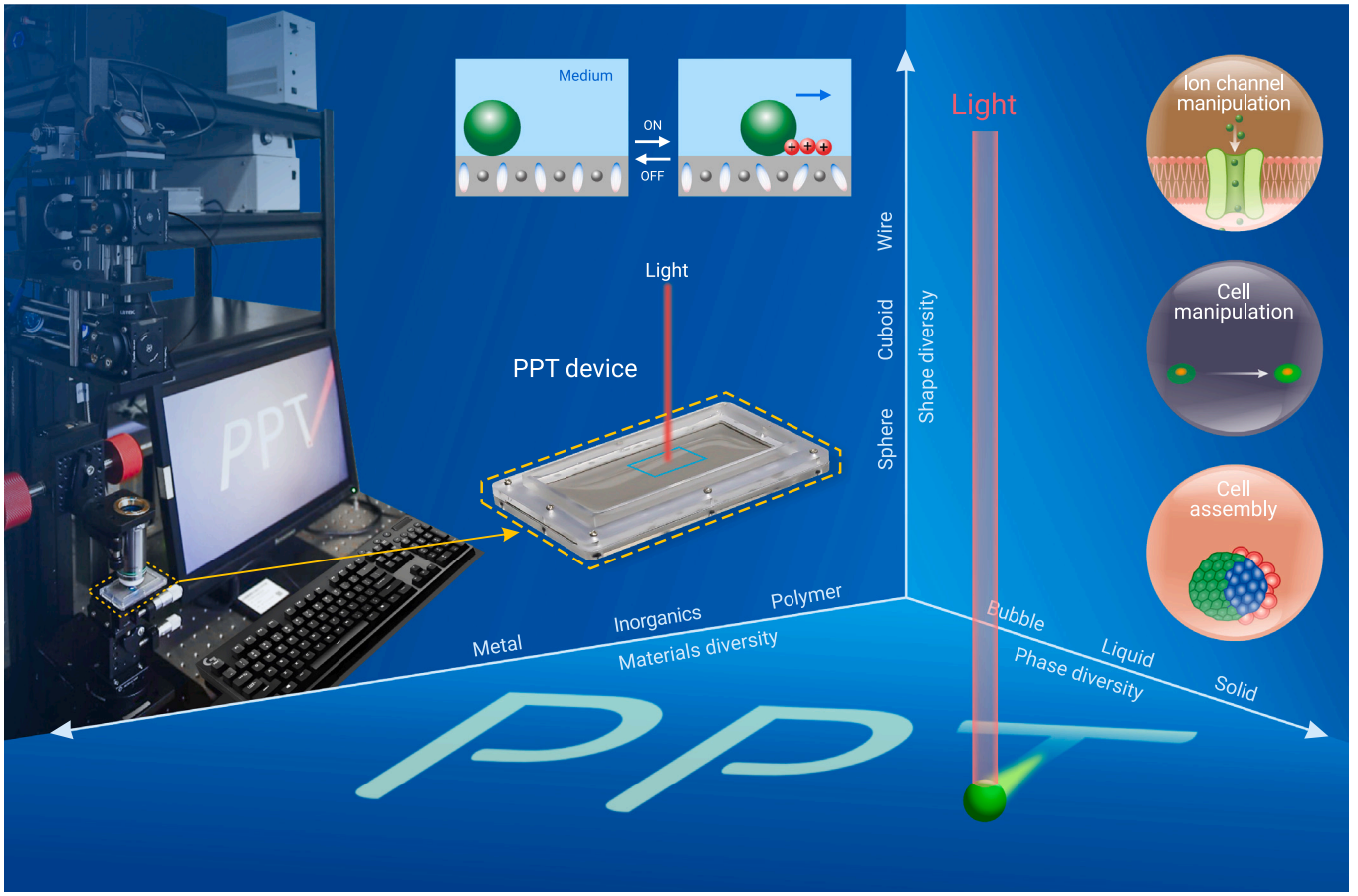

PUBLIC SUMMARY

- Photopyroelectric tweezers that combine the advantages of light and electric fields have been firstly achieved.
- Photopyroelectric tweezers induce a large driving force (~μN) when exposed to low-intensity near-infrared irradiation.
- Photopyroelectric tweezers enable remote and programmable manipulation of objects with diverse materials (polymer, inorganic, and metal), different phases (bubble, liquid, and solid), and various geometries (sphere, cuboid, and wire).
- Photopyroelectric tweezers are not only adaptive to various media but also generic to portable macroscopic manipulation platforms and microscopic manipulation systems, enabling cross-scale (size: μm to cm) manipulations.
- Photopyroelectric tweezers allow for diverse applications in robotic and biomedical domains including manipulating hydrogel robots, sorting particles, assembling living cells, manipulating a single cell, and stimulating cells.

OPEN ACCESS

REPORT

The Innovation

Photopyroelectric tweezers for versatile manipulation

Fang Wang,[1,5] Cong Liu,[1,2,5] Zhengjin Dai,[1,4,5] Weizhong Xu,[1] Xinyue Ma,[1] Yufeng Gao,[1] Xuewu Ge,[4] Wei Zheng,[1] and Xuemin Du[1,2,3,*]

[1]Center for Intelligent Biomedical Materials and Devices (IBMD), Shenzhen Institute of Advanced Technology (SIAT), Chinese Academy of Sciences (CAS), Shenzhen 518055, China

[2]University of Chinese Academy of Sciences, Beijing 100049, China

[3]The Key Laboratory of Biomedical Imaging Science and System, Chinese Academy of Sciences, Shenzhen 518055, China

[4]Department of Polymer Science and Engineering, University of Science & Technology of China, Hefei 230026, China

[5]These authors contributed equally

*Correspondence: xm.du@siat.ac.cn

Received: June 12, 2024; Accepted: November 22, 2024; Published Online: December 12, 2024; https://doi.org/10.1016/j.xinn.2024.100742

© 2024 The Author(s). Published by Elsevier Inc. on behalf of Youth Innovation Co., Ltd. This is an open access article under the CC BY-NC-ND license (http://creativecommons.org/licenses/by-nc-nd/4.0/).

Citation: Wang F., Liu C., Dai Z., et al., (2025). Photopyroelectric tweezers for versatile manipulation. The Innovation **6(1)**, 100742.

Optical tweezers and related techniques offer extraordinary opportunities for research and applications in physical, biological, and medical fields. However, certain critical requirements, such as high-intensity laser beams, sophisticated electrode designs, additional electric sources, or low-conductive media, significantly impede their flexibility and adaptability, thus hindering their practical applications. Here, we report innovative photopyroelectric tweezers (PPT) that combine the advantages of light and electric field by utilizing a rationally designed photopyroelectric substrate with efficient and durable photo-induced surface charge-generation capability, enabling diverse manipulation in various working scenarios. These PPTs allow for remote and programmable manipulation of objects with diverse materials (polymer, inorganic, and metal), different phases (bubble, liquid, and solid), and various geometries (sphere, cuboid, and wire). Furthermore, the PPT is not only adaptable to high-conductivity media but also applicable to both portable macroscopic manipulation platforms and microscopic manipulation systems, enabling cross-scale manipulations for solid objects, liquid droplets, and biological samples. The high-level flexibility and adaptability of the PPT extend to broad applications in manipulating hydrogel robots, sorting particles, assembling cells, and stimulating cells. By surpassing the limitations of conventional tweezers, the PPT bridges the gap between macroscopic and microscopic manipulations, offering a revolutionary tool in robotics, colloidal science, biomedical fields, and beyond.

INTRODUCTION

Remote and non-invasive manipulation techniques have led to significant breakthroughs in various fields including colloidal science, robotics, medicine, and biology.[1-6] Over recent decades, these manipulation techniques have developed into diverse forms, such as acoustic tweezers,[7] magnetic tweezers,[8] and electrostatic tweezers,[9,10] which have proven to be valuable tools for manipulating micro/nanoparticles, microrobots, and liquid droplets, among others. These tweezers have all evolved from their predecessor, optical tweezers, which were invented by Ashkin et al. in 1986.[11] Optical tweezers, as a revolutionary technique, have been extensively investigated for trapping particles (with sizes <30 μm, such as colloids, cells, molecules, etc.) at the micro- to nanoscale using optical gradient forces (piconewtons, $\sim10^{-12}$ N).[1,4,12,13] Despite their significant progress, optical tweezers still have inherent limitations due to the critical requirements of tightly focused high-intensity laser beams ($\sim1 \times 10^{7}$ mW mm^{-2}) and high refractive index contrast between the trapped objects and the surrounding liquid media, which can damage fragile objects and significantly reduce manipulation diversity.[1,5,13]

To address the challenges mentioned above, optical tweezers have been combined with various photosensitive materials, including plasmonic, opto-thermal/refrigerative, and semiconductor substrates, resulting in the development of alternative technologies such as plasmonic tweezers,[14,15] opto-thermal/refrigerative tweezers,[16-18] opto-thermoelectric tweezers,[19-21] and optoelectronic tweezers.[22-29] Among these technologies, optoelectronic tweezers (OET) have gained significant attention due to their ability to produce non-uniform electric fields in the liquid medium, based on the photoconductive effect of semiconductor substrates. These light-induced non-uniform electric fields create substantial dielectrophoresis forces (nanonewtons, $\sim10^{-9}$ N), allowing for the manipulation of nanoscale and microscale particles with lower light power density (~10 mW mm^{-2}), which is otherwise impossible using other optical tweezers.[2,3,30] However, such combination with the semiconductor substrates also brings undesired issues.[2,31,32] Firstly, the production of non-uniform electric fields in conventional OET is vitally dependent on a sophisticated semiconductor substrate sandwiched between top and bottom indium tin oxide electrodes biased with an external electric source, which not only leads to a narrow manipulation area ($\sim$<2 cm^2), but also complicates the manipulation platforms. Secondly, these semiconductor substrates can only work in low-conductivity media (<0.001 S cm^{-1}) owing to their finite photoconductivity, thus creating insufficient trapping forces. Thirdly, these substrates are easily contaminated by the manipulated particles due to non-specific bonding, thereby affecting the performance of OET. These issues significantly hinder the flexibility and adaptability of OET, thus impeding their practical applications.[2,13,33]

Here, we first report a new concept of a photopyroelectric tweezer (PPT) that combines the dual advantages of light and electric fields, imparting unrivaled flexibility and adaptability for diverse object manipulation in various working scenarios. Different from previous tweezers (Figures 1A–1F and S1), the PPT utilizes a rationally designed photopyroelectric substrate that efficiently and durably generates surface charges when exposed to low-intensity near-infrared (NIR) (as low as $\sim$8.3 mW mm^{-2}) irradiation,[34,35] thereby inducing a large driving force (micronewtons, as large as $\sim4.6 \times 10^{-5}$ N) without the need for high-intensity laser beam, sophisticated electrode designs, and additional electric sources. Such PPT allows for remotely and programmably manipulating objects with diverse materials (polymer, inorganic, and metal), different phases (bubble, liquid, and solid), and various geometries (sphere, cuboid, and wire) (Figures 1G, 1H, and S2–S4; Video S1). Moreover, this PPT is not only adaptive to various media with wide-range conductivities (0.001–91.0 mS cm^{-1}) but also applicable to portable macroscopic manipulation platforms and microscopic manipulation systems with on-demand manipulating areas (12.5–96.0 cm^2; Figures 1B, S5, and S6), enabling cross-scale manipulations for solid objects ranging from 5 μm to 2.5 mm, liquid droplets ranging from 1 pL to 10 mL (Video S2), and biological samples from single cells to cell assemblies (Video S3). Such high-level flexibility and adaptability of the PPT extends to diverse applications in robotic and biomedical domains, including manipulating hydrogel robots, sorting particles, assembling living cells, manipulating single cells, and stimulating cells. The PPT overcomes the limitations inherent in conventional tweezers, bridging the gap between the macroscopic and microscopic manipulations, and suggests promising potentials for broad applications in robotics, colloidal, biomedical fields, and beyond.

RESULTS AND DISCUSSION

Design of PPT

The PPT platform comprises two key components: a NIR laser light source and a PPT device, which contains a liquid medium and a photopyroelectric substrate (Figures 1A and 1B). In particular, the photopyroelectric substrate consists of a superhydrophobic ferroelectric polymer layer made of Ga-In liquid metal microparticle-embedded poly(vinylidene fluoride-*co*-trifluoroethylene) (LMPs/P(VDF-TrFE)) composites, and a lubricant-infused slippery layer (Figures 1C and S7; see supplemental materials and methods). Here, the polymer layer serves to generate real-time surface charges based on the photopyroelectric effect, whereas the lubricant layer reduces motion resistance, suppresses contamination, and prevents the charge screening effect caused by conductive media, as previously proposed in our work.[34] When the photopyroelectric substrate is exposed to NIR light irradiation, the embedded LMPs in the polymer

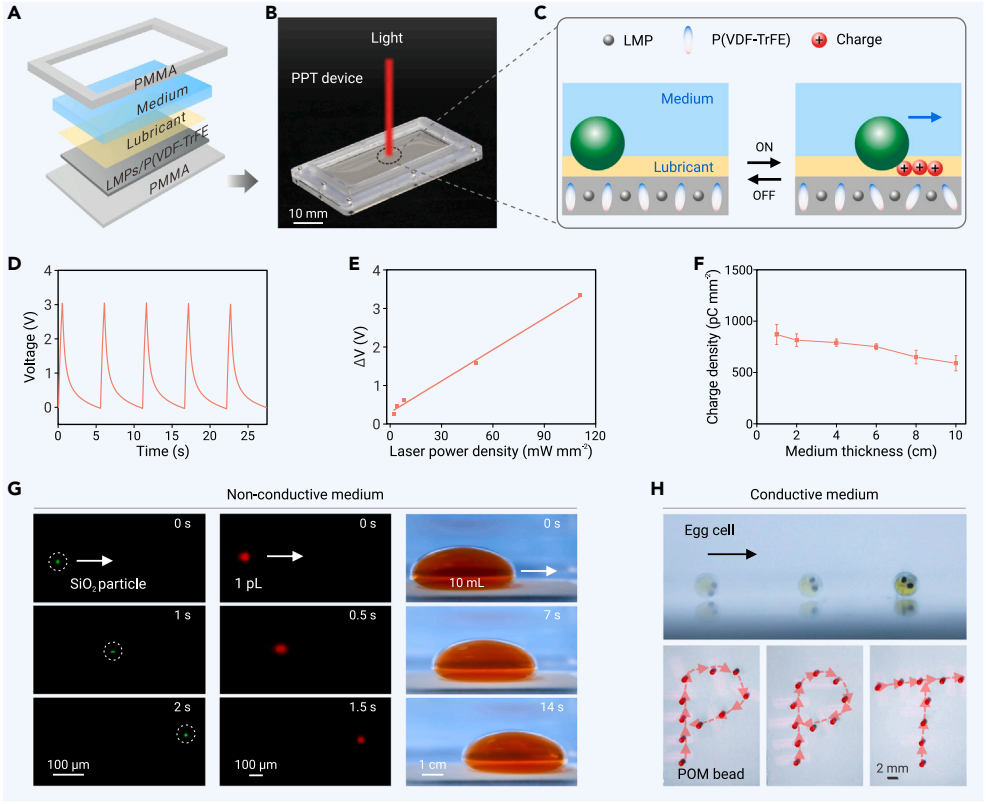

Figure 1. PPT design (A) Schematic illustration of PPT device consisting of a liquid medium, a lubricant layer, and an LMPs/P(VDF-TrFE) film sandwiched between top and bottom poly (methyl methacrylate) (PMMA) slides. (B) Photograph of the PPT platform containing a NIR laser light source and a portable PPT device with a large manipulation area of 12.5 cm^2. Scale bar: 10 mm. (C) Schematic illustration of the PPT platform for object manipulation based on the photopyroelectric effect. (D) The output voltage of the PPT device upon exposure to NIR irradiation (power density: 100 mW mm^{-2}, frequency: 0.5 s ON and 5 s OFF). (E) The voltage changes increase from 0.26 to 3.34 V with an increase in the laser power density from 2 to 111 mW mm^{-2}. (F) The light-induced charge density of the PPT shows slight variation from 870 to 590 pC mm^{-2} by increasing the medium (silicone oil) thickness from 1 to 10 cm. Error bars are calculated from five independent measurements. (G) Manipulating 5-μm SiO_2 particle, 1 pL water droplet, and 10 mL water droplet in a non-conductive medium (silicone oil, Video S2). (H) Manipulating a live medaka egg cell (1 mm diameter), and the time-lapse trajectory of 1-mm POM bead in a conductive medium (water, Videos S3 and S4).

composites rapidly convert light into a local temperature increase, leading to a decrease in P(VDF-TrFE) polarization and thus generating surface charges as compensation at the irradiated area (Figures 1C and S8). Upon turning off the light irradiation, the temperature decreases, causing an increase in the P(VDF-TrFE) polarization to its initial status and thus leading to the disappearance of the surface charges. This charge generation capability is demonstrated by the temporary voltage output, which increases with an increase in the irradiated laser power density (Figures 1D, 1E, S9, and S10). It is worth noting that this robust charge generation capability shows negligible variation either in various media of large-range thicknesses (1–10 cm) or wide-range conductivities (1.16–91 mS cm^{-1}; Figures 1F and S11). Such results suggest that the PPT not only eliminates the need for sophisticated electrode designs and additional electric sources, but also eliminates the undesired charge screening effect caused by the high-conductivity media, which was otherwise impossible in previous works.[22,36–38]

Manipulation mechanism

We next conducted a model to elucidate the underlying mechanism of PPT-induced object dynamics (see supplemental materials). As shown in Figure 2A, bringing a NIR laser spot close to an object situated on the photopyroelectric substrate immersed in a non-conductive medium results in a surface

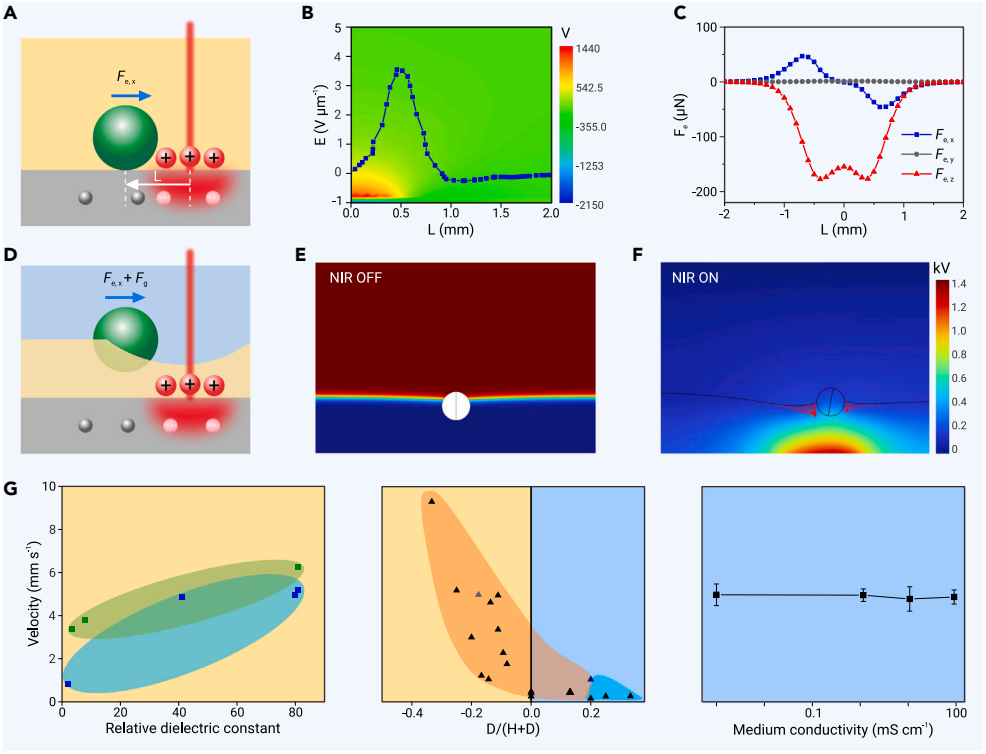

Figure 2. Mechanism of PPT (A) Schematic illustration of manipulating an object with PPT in a non-conductive medium, where $F_{e,x}$ determines the object dynamics. (B) The electrical potential mapping and distribution along the L (x axis distance from the irradiated spot center to the object center) direction upon exposure to NIR irradiation (L-direction width of the laser spot: 0.5 mm). (C) The $F_{e,x}$, $F_{e,y}$, and $F_{e,z}$ can be tuned by changing L. (D) Schematic illustration of manipulating an object with PPT in a conductive medium, where $F_{e,x}$ and F_g determine the object dynamics. (E) The side view of the aimed object located at the conductive medium-lubricant interface before being exposed to NIR irradiation. (F) The electrical potential mapping and distribution at the side view of the aimed object situated at the medium-lubricant interface when exposed to NIR irradiation. The light-induced T_x exerts on the conductive medium-lubricant interface around the aimed object and its immersed part in the lubricant layer. (G) Phase diagram showing the object dynamic behaviors in non-conductive and conductive media, along with changes in the relative dielectric constant of objects (left: green dot, solid objects; blue dot, liquid droplets), the object position in the conductive medium (middle: orange area, solid objects situated at the medium-lubricant interface; blue area, solid objects situated on the medium-lubricant interface), and the medium conductivity. D is the distance from the medium-lubricant interface to the object center. H is the thickness of the lubricant layer. Error bars are calculated from five independent measurements.

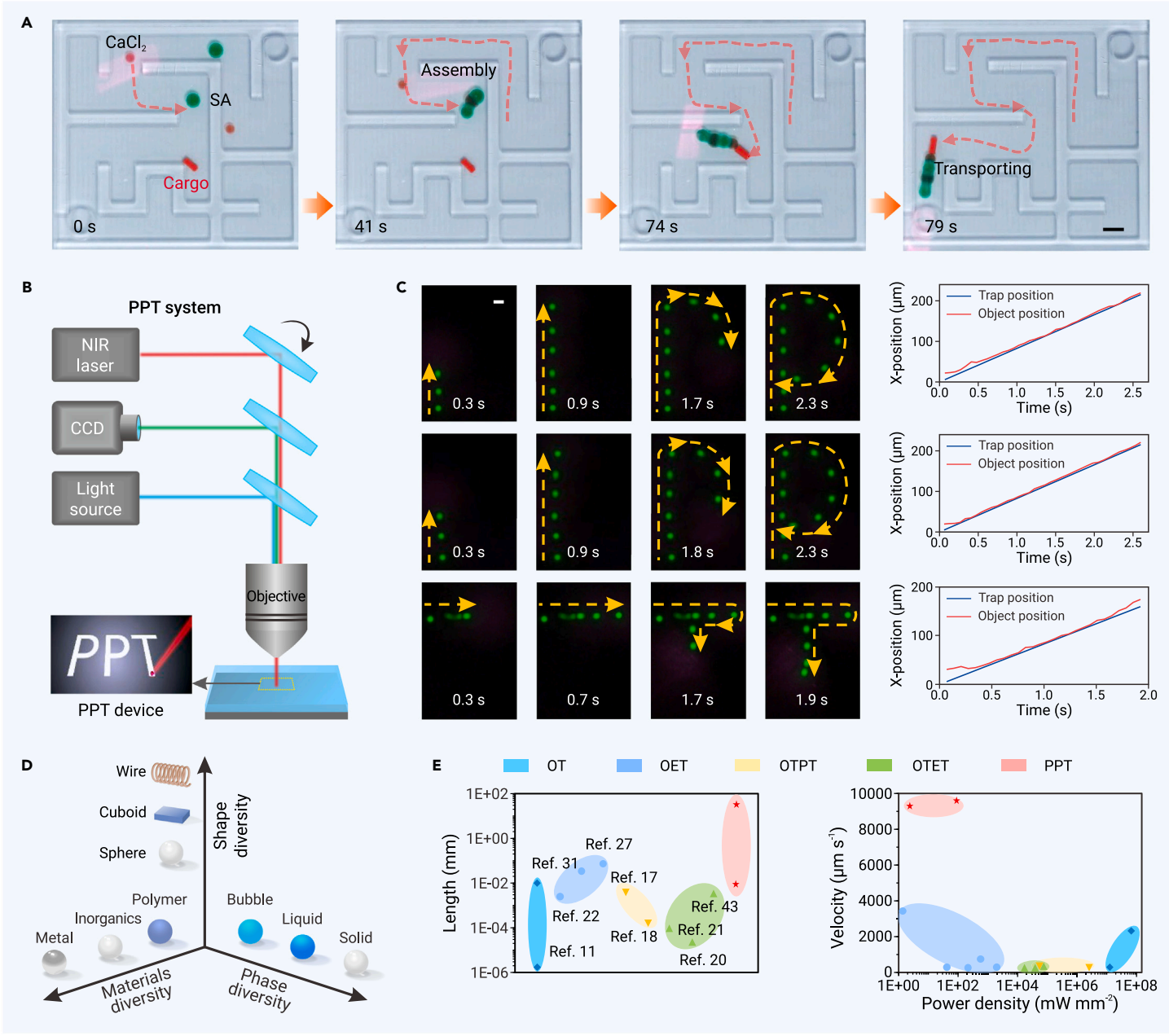

Figure 3. PPT for cross-scale object manipulation (A) Manipulating a 1-μL SA droplet and a 0.5-μL $CaCl_2$ droplet first assembled into a hydrogel-chain robot, then crossing a maze and transporting the red solid cargo in a closed microfluidic chip filled with a silicone oil medium. Scale bar: 2 mm. (B) Schematic illustration of the PPT-integrated microscopic system for manipulating microparticles. (C) PPT system for programmably manipulating 5-μm polystyrene (PS) particles in a silicone oil medium. The yellow lines indicate the time-lapse trajectory of the PS particles, which move along the pre-set "PPT" path. The spatial and temporal resolution of the PPT can be revealed by tracking both the irradiated spot (pre-set velocity: 105 μm s^{-1}) and the particle central positions. Scale bar: 10 μm. (D) General capability of the PPT for manipulating objects with diverse materials, phases, and shapes. (E) Comparison of the PPT performances with the reported optical tweezers (OT), OET, opto-thermophoretic tweezers (OTPT), and opto-thermoelectric tweezers (OTET).

charge-induced large non-uniform electric field at the irradiation area (Figure 2B), which induces Maxwell stress tensors (T_{ij}) on the object that can be expressed as[39]

$$T_{ij} = \varepsilon_0 \varepsilon_r \left(E_i E_j - \frac{1}{2} \delta_{ij} E^2 \right) \quad \text{(Equation 1)}$$

where $\boldsymbol{T}$, ε_0, ε_r, δ_{ij}, and E are the Maxwell stress tensor, the dielectric constant of vacuum, the relative dielectric constant of the aimed object, the Kronecker delta notation, and the electric field intensity, respectively. Maxwell stress tensor distribution in the x direction (T_x) exerting on the object is obtained by a finite element analysis, as shown in Figure S12, suggesting that the T_x centralizes on both front and rear surfaces of the object, with a greater magnitude on the front surface near the area subjected to irradiation. The integration of the Maxwell stress tensors yields the driving force F_e on the aimed object, which can be expressed as

$$\mathbf{F}_e = \iint \mathbf{T} \cdot \mathbf{n} dS \quad \text{(Equation 2)}$$

where $\boldsymbol{n}$ is the surface unit normal and dS is an elementary surface area of the object. The simulation results of the COMSOL Multiphysics suggest that the F_e components $F_{e,y}$ are negligible due to the symmetric Maxwell stress tensors in the y direction (T_y), and thus the combined $F_{e,x}$ and $F_{e,z}$ determine the object dynamics.[9,35] Notably, when the NIR laser spot moves to L = 0.7 mm, $F_{e,x}$ increases to its maximum value of 46 μN, which is six and three orders of magnitude higher than that of optical tweezers and OET, respectively (Figure 2C).[2] In a conductive medium, the interaction between the light-induced T_x and the conductive medium-lubricant interface plays a crucial role in contrast to a non-conductive medium (Figure 2D).[40] Such interaction creates a potential well (x axis component, F_g) and $F_{e,x}$, thus exerting control over the object dynamics (Figures 2E, 2F, S13 and S14). These results indicate that the driving forces exposed to the aimed

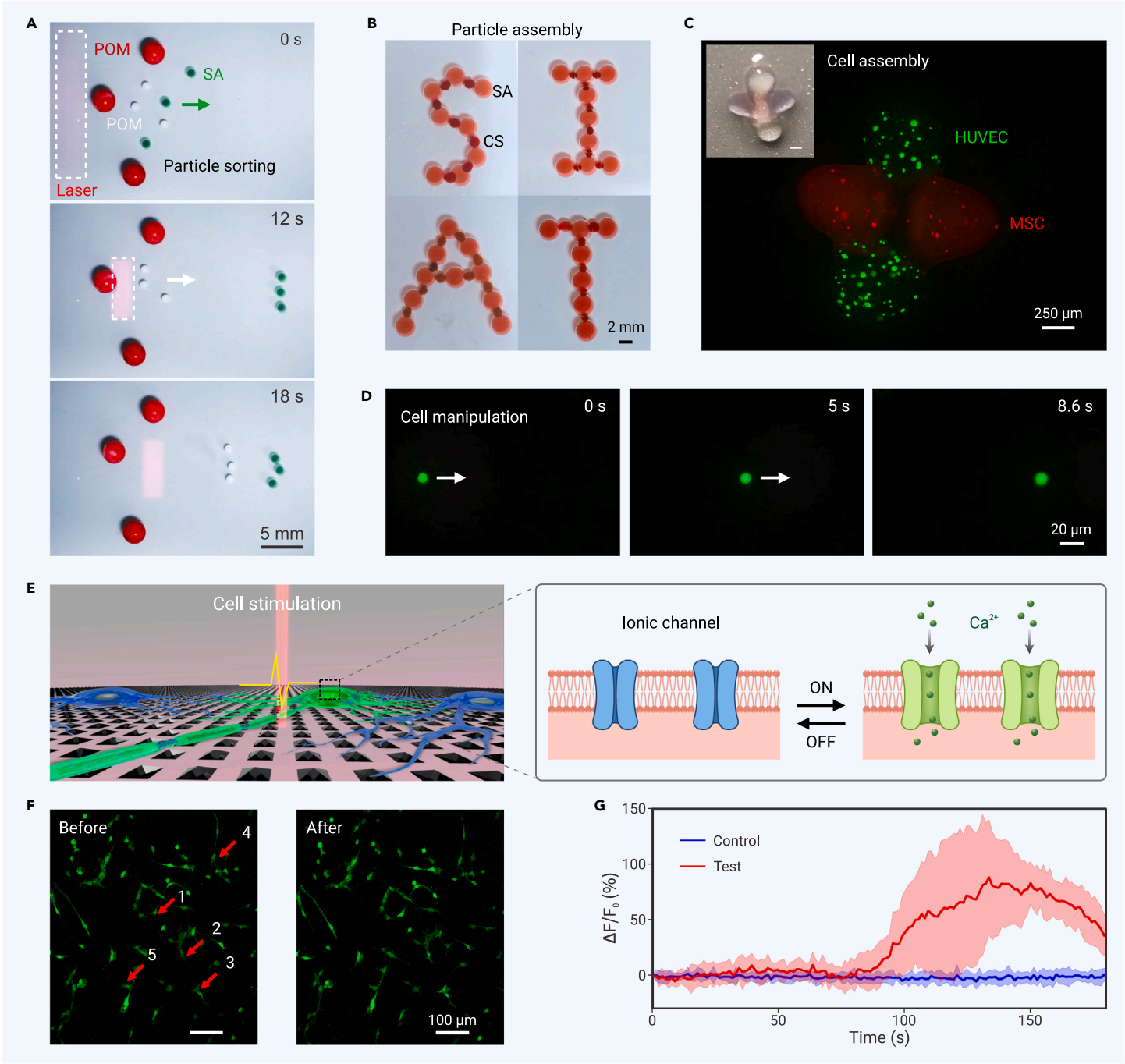

Figure 4. PPT for various applications (A) Sorting SA hydrogel and POM particles in a silicone oil medium by adjusting the laser power density of the NIR irradiation from 5 to 28 mW mm^{-2}. Scale bar: 5 mm. (B) Assembly of SA and CS hydrogel beads into the letters "S," "I," "A," and "T" in a silicone oil medium. Scale bar: 2 mm. (C) Non-invasive assembly of human umbilical vein endothelial cells (HUVECs) and mesenchymal stem cells (MSCs) in a silicone oil medium. Scale bar: 250 μm. (D) Non-invasive manipulation of a live PC 12 cell in cell culture medium. Scale bar: 20 μm. (E) Schematic illustration of manipulating ionic channels of cells in cell culture medium. (F) Fluorescent images of PC 12 cells before and after the NIR irradiation. Scale bar: 100 μm. (G) Ca^{2+} signals of cells for the control and test. Error bars are calculated from five independent measurements.

objects can be facilely regulated by varying the electric field (i.e., laser power density), the aimed object dielectric constant and size, or the relative position between the object and the laser spot (L, in the non-conductive medium; $D/(H + D)$, in the conductive medium).

We further experimentally demonstrate that the object dynamics are consistent with the simulation results (Figure 2G). As shown in Figures S15–S17 and Video S5, polyformaldehyde (POM), glass, and metal balls can be facilely manipulated on the photopyroelectric substrate in a non-conductive medium, and the average velocity increases with higher laser power density, larger relative dielectric constant of the object, and smaller object size. Conversely, when placed on control substrates without photopyroelectric effect, these balls remain immobile due to the absence of a light-induced driving force (Figure S18). In addition, we have also elucidated that POM, glass, and hydrogel balls can be similarly manipulated in a conductive medium (Figure S19; Video S6). In contrast to their behavior in the non-conductive medium, these balls float at the conductive medium-lubricant interface. Furthermore, their average velocity increases with increasing laser power density, or decreasing $D/(H + D)$, which can be achieved by modifying the object size, the thickness of the lubricant layer (H), or the immersed depth of the object in the lubricant layer (D) (Figures S16, S20 and S21). Moreover, the PPT exhibits adaptability to various media with a wide range of conductivities, ranging from 0.001 to 91 mS cm^{-1}. These results suggest that the conductive medium does not significantly influence the object dynamics.

PPT for diverse manipulation

Leveraging its flexibility and adaptability, the PPT enables precise manipulation in both macroscopic and microscopic scenarios. As shown in Figure S22A and

Video S7, a green droplet containing sodium alginate (SA) (4 wt %) can be manipulated and then fused with a red droplet containing calcium chloride ($CaCl_2$) (1 M) in a silicone oil medium, leading to the rapid formation of a physically crosslinked SA hydrogel-bead robot. These hydrogel-bead robots can be precisely assembled into a hydrogel-chain robot by selectively manipulating a droplet stepwise using a portable laser pointer (Figure S22B; Video S8). Interestingly, the hydrogel-chain robot exhibits caterpillar-like behavior, successfully navigating through a maze and transporting a red cargo to the destination within a closed microfluidic chip owing to the high spatial and temporal resolution of the PPT (Figure 3A; Video S9). Furthermore, three SA hydrogel-bead robots can be collectively manipulated by a single laser beam, resembling the behavior of an ant colony in nature (Figure S22C; Video S10). In addition, both airflow and liquid flow can also be facilely manipulated (Figure S23), which holds great promise for applications including gas transport or fluid collection.[41,42] Beyond precise manipulation in a non-conductive medium, six POM balls can also be manipulated and patterned into a triangle shape in an aqueous medium (Figure S24).

In addition to its macro-scale manipulation capabilities, the PPT platform is also adaptable for integration with a microscopic system for micro-scale object manipulation. As shown in Figures 3B and S25, the homemade microscopic manipulation system (i.e., PPT system) consists of three core components: software for programming the scanning speed and path of the NIR laser spot, a fluorescent light source and CCD for fluorescence imaging of the manipulated object, and the PPT device. Similar to macro-scale manipulation, various microparticles can be facilely manipulated in both non-conductive and conductive media, and their velocities and motion paths can be pre-programmed. As shown in Figure 3C, a single polystyrene particle with a diameter of 5 μm can move precisely along the pre-set "PPT" path with a pre-set velocity of 105 μm s^{-1} in a silicone oil medium (Video S11). Furthermore, SiO_2 particles with diameters of 5 and 20 μm can also be manipulated in an aqueous medium with a pre-set velocity of 80 μm s^{-1} (Figure S26). Note that these particles would not contaminate the photopyroelectric substrate owing to the rational design of the lubricant layer, which prevents bonding between the aimed object and the substrate. Compared with previous tweezers,[11,17,18,20–23,27,31,43–50] the PPT not only demonstrates overwhelmingly collective performances including generality to objects with diverse materials (polymer, inorganic, and metal), different phases (bubble, liquid, and solid), and various geometries (sphere, cuboid, and wire), as shown in Figure 3D, but also imparts cross-scale manipulation of objects ranging from 5 μm to 50 mm, achieving high velocities of 9.3 × 10^3 to 9.6 × 10^3 μm s^{-1} solely using low laser power density ranging from 8.3 to 111 mm^{-2} (Figure 3E; Tables S1 and S2), overcoming the inherent limitations in conventional tweezers.

PPT for various applications

We further harness the robust PPT for broad application scenarios. Firstly, we demonstrate that the PPT enables particle sorting according to their relative dielectric constant or size differences. Figure 4A and Video S12 shows that three green SA hydrogel particles (diameter: 0.9 mm) and six POM particles with different size (diameter: 0.9 and 2.5 mm) were mixed together. By applying a low laser power density (5 mW mm^{-2}), three green SA hydrogel particles were first sorted by a single laser beam because of their large interaction with the tweezer. After increasing the laser power density to 28 mW mm^{-2}, three white small-size POM particles were then manipulated to a specific position, while the other three red large-size POM particles were left at their initial position because their interaction with the tweezer could not overcome the resistance from the medium and the photopyroelectric substrate. Furthermore, the PPT can be used for precise and remote manipulation of large SA and small chitosan (CS) hydrogel robots to assembly into a "SIAT" pattern (Figure 4B).

In addition, the PPT allows for biocompatible manipulation for constructing cell assemblies by adding primary human umbilical vein endothelial cells and mesenchymal stem cells into the hydrogel particles (Figure 4C). Moreover, the PPT can manipulate a single live PC 12 cell in a non-invasive manner (Figure 4D). Such robust capability offers an innovative platform for investigating cell assembly and organoids. Note that the PPT can be used for stimulating PC 12 cells unprecedentedly (Figure 4E). As shown in Figure 4F, PC 12 cells were cultured on the photopyroelectric substrate in the absence of a lubricant layer. After 3 days, the cells adhered onto the substrate with high density, indicating the good biocompatibility of the substrate. To investigate the interaction between cell activities and the PPT, we further perform dynamic calcium (Ca^{2+}) imaging of PC 12 cells cultured on the substrate (Figures 4F and 4G). For PC 12 cells on the photopyroelectric substrate, the fluorescence increases upon NIR light irradiation, suggesting that the PPT induces the ion channels to open in the cells owing to the unique photopyroelectric effect.[34,35,51-56] On the contrary, the fluorescence shows no change for PC 12 cells on the control substrate without photopyroelectric effect, indicating negligible cell activities (Figures S27 and S28). These results suggest that the PPT could open new avenues for next-generation manipulation techniques, bringing an innovative tool in the fields of robots, colloidal science, organoids, tissue engineering, and neuromodulation.[57–63]

CONCLUSION

In summary, we first propose a novel PPT that combines the dual advantages of light and electric field, imparting unrivaled flexibility and adaptability for diverse object manipulation based on the photopyroelectric effect. Eliminating the need for high-intensity laser beams, sophisticated electrode designs, and additional electric sources, this innovative PPT enables remote and programmable manipulation of objects with diverse materials (polymer, inorganic, and metal), different phases (bubble, liquid, and solid), various geometries (sphere, cuboid, and wire), and cross-scale sizes (μm to cm). Together with its high adaptability to various media and generality to both macroscopic manipulation platforms and microscopic manipulation systems, the PPT finds diverse practical applications in manipulating hydrogel robots, sorting particles, assembling different cells, manipulating a single cell, and stimulating cells. We envision that the PPT, bridging the gap between macroscopic and microscopic manipulations, will offer unprecedented opportunities in robotics, material science, and biomedical fields.

REFERENCES

1. Ozcelik, A., Rufo, J., Guo, F., et al. (2018). Acoustic tweezers for the life sciences. Nat. Methods ***15***(12): 1021–1028. https://doi.org/10.1038/s41592-018-0222-9.
2. Zhang, S., Xu, B., Elsayed, M., et al. (2022). Optoelectronic tweezers: a versatile toolbox for nano-/micro-manipulation. Chem. Soc. Rev. ***51***(22): 9203–9242. https://doi.org/10.1039/D2CS00359G.
3. Chen, Z., Li, J., and Zheng, Y. (2022). Heat-mediated optical manipulation. Chem. Rev. ***122***(3): 3122–3179. https://doi.org/10.1021/acs.chemrev.1c00626.
4. Bustamante, C.J., Chemla, Y.R., Liu, S., et al. (2021). Optical tweezers in single-molecule biophysics. Nat. Rev. Methods Primers ***1***(1): 25. https://doi.org/10.1038/s43586-021-00021-6.
5. Neuman, K.C., and Nagy, A. (2008). Single-molecule force spectroscopy: optical tweezers, magnetic tweezers and atomic force microscopy. Nat. Methods ***5***(6): 491–505. https://doi.org/10.1038/nmeth.1218.
6. Wu, X., Ehehalt, R., Razinskas, G., et al. (2022). Light-driven microdrones. Nat. Nanotechnol. ***17***(5): 477–484. https://doi.org/10.1038/s41565-022-01099-z.
7. Yang, Y., Yang, Y., Liu, D., et al. (2023). In-vivo programmable acoustic manipulation of genetically engineered bacteria. Nat. Commun. ***14***(1): 3297. https://doi.org/10.1038/s41467-023-38814-w.
8. Bausch, A.R., Möller, W., and Sackmann, E. (1999). Measurement of local viscoelasticity and forces in living cells by magnetic tweezers. Biophys. J. ***76***(1): 573–579. https://doi.org/10.1016/S0006-3495(99)77225-5.
9. Jin, Y., Xu, W., Zhang, H., et al. (2022). Electrostatic tweezer for droplet manipulation. Proc. Natl. Acad. Sci. USA ***119***(2): e2105459119. https://doi.org/10.1073/pnas.2105459119.
10. Fan, D.L., Zhu, F.Q., Cammarata, R.C., et al. (2011). Electric tweezers. Nano Today ***6***(4): 339–354. https://doi.org/10.1016/j.nantod.2011.05.003.
11. Ashkin, A., Dziedzic, J.M., Bjorkholm, J.E., et al. (1986). Observation of a single-beam gradient force optical trap for dielectric particles. Opt. Lett. ***11***(5): 288–290. https://doi.org/10.1364/OL.11.000288.
12. Ashkin, A., and Dziedzic, J.M. (1987). Optical trapping and manipulation of viruses and bacteria. Science ***235***(4795): 1517–1520. https://doi.org/10.1126/science.3547653.
13. Dholakia, K., Drinkwater, B.W., and Ritsch-Marte, M. (2020). Comparing acoustic and optical forces for biomedical research. Nat. Rev. Phys. ***2***(9): 480–491. https://doi.org/10.1038/s42254-020-0215-3.
14. Grigorenko, A.N., Roberts, N.W., Dickinson, M.R., et al. (2008). Nanometric optical tweezers based on nanostructured substrates. Nat. Photonics ***2***(6): 365–370. https://doi.org/10.1038/nphoton.2008.78.
15. Righini, M., Zelenina, A.S., Girard, C., et al. (2007). Parallel and selective trapping in a patterned plasmonic landscape. Nat. Phys. ***3***(7): 477–480. https://doi.org/10.1038/nphys624.
16. Lin, L., Peng, X., Mao, Z., et al. (2016). Bubble-pen lithography. Nano Lett. ***16***(1): 701–708. https://doi.org/10.1021/acs.nanolett.5b04524.
17. Lin, L., Peng, X., Wei, X., et al. (2017). Thermophoretic tweezers for low-power and versatile manipulation of biological cells. ACS Nano ***11***(3): 3147–3154. https://doi.org/10.1021/acsnano.7b00207.
18. Li, J., Chen, Z., Liu, Y., et al. (2021). Opto-refrigerative tweezers. Sci. Adv. ***7***(26): eabh1101. https://doi.org/10.1126/sciadv.abh1101.

19. Lin, L., Zhang, J., Peng, X., et al. (2017). Opto-thermophoretic assembly of colloidal matter. Sci. Adv. ***3***(9): e1700458. https://doi.org/10.1126/sciadv.1700458.
20. Liu, Y., Lin, L., Bangalore Rajeeva, B., et al. (2018). Nanoradiator-mediated deterministic opto-thermoelectric manipulation. ACS Nano ***12***(10): 10383–10392. https://doi.org/10.1021/acsnano.8b05824.
21. Lin, L., Wang, M., Peng, X., et al. (2018). Opto-thermoelectric nanotweezers. Nat. Photonics ***12***(4): 195–201. https://doi.org/10.1038/s41566-018-0134-3.
22. Chiou, P.Y., Ohta, A.T., and Wu, M.C. (2005). Massively parallel manipulation of single cells and microparticles using optical images. Nature ***436***(7049): 370–372. https://doi.org/10.1038/nature03831.
23. Jamshidi, A., Pauzauskie, P.J., Schuck, P.J., et al. (2008). Dynamic manipulation and separation of individual semiconducting and metallic nanowires. Nat. Photonics ***2***(2): 86–89. https://doi.org/10.1038/nphoton.2007.277.
24. Wang, W., Lin, Y.-H., Guan, R.-S., et al. (2009). Bulk-heterojunction polymers in optically-induced dielectrophoretic devices for the manipulation of microparticles. Opt. Express ***17***(20): 17603–17613. https://doi.org/10.1364/OE.17.017603.
25. Yang, S.-M., Yu, T.-M., Huang, H.-P., et al. (2010). Dynamic manipulation and patterning of microparticles and cells by using TiOPc-based optoelectronic dielectrophoresis. Opt. Lett. ***35***(12): 1959–1961. https://doi.org/10.1364/OL.35.001959.
26. Zhang, S., Liu, Y., Juvert, J., et al. (2016). Use of optoelectronic tweezers in manufacturing—accurate solder bead positioning. Appl. Phys. Lett. ***109***(22): 221110. https://doi.org/10.1063/1.4971348.
27. Zhang, S., Juvert, J., Cooper, J.M., et al. (2016). Manipulating and assembling metallic beads with Optoelectronic Tweezers. Sci. Rep. ***6***(1): 32840. https://doi.org/10.1038/srep32840.
28. Zhang, S., Scott, E.Y., Singh, J., et al. (2019). The optoelectronic microrobot: A versatile toolbox for micromanipulation. Proc. Natl. Acad. Sci. USA ***116***(30): 14823–14828. https://doi.org/10.1073/pnas.1903406116.
29. Zhang, S., Elsayed, M., Peng, R., et al. (2021). Reconfigurable multi-component micromachines driven by optoelectronic tweezers. Nat. Commu. ***12***(1): 5349. https://doi.org/10.1038/s41467-021-25582-8.
30. Juan, M.L., Righini, M., and Quidant, R. (2011). Plasmon nano-optical tweezers. Nat. Photonics ***5***(6): 349–356. https://doi.org/10.1038/nphoton.2011.56.
31. Hsu, H.-Y., Ohta, A.T., Chiou, P.-Y., et al. (2010). Phototransistor-based optoelectronic tweezers for dynamic cell manipulation in cell culture media. Lab Chip ***10***(2): 165–172. https://doi.org/10.1039/B906593H.
32. Wu, M.C. (2011). Optoelectronic tweezers. Nat. Photonics ***5***(6): 322–324. https://doi.org/10.1038/nphoton.2011.98.
33. Kumar, A., Williams, S.J., Chuang, H.-S., et al. (2011). Hybrid opto-electric manipulation in microfluidics—opportunities and challenges. Lab Chip ***11***(13): 2135–2148. https://doi.org/10.1039/C1LC20208A.
34. Wang, F., Liu, M., Liu, C., et al. (2022). Light-induced charged slippery surfaces. Sci. Adv. ***8***(27): eabp9369. https://doi.org/10.1126/sciadv.abp9369.
35. Wang, F., Liu, M., Liu, C., et al. (2023). Light control of droplets on photo-induced charged surfaces. Natl. Sci. Rev. ***10***(1): nwac164. https://doi.org/10.1093/nsr/nwac164.
36. Nasti, G., Coppola, S., Vespini, V., et al. (2020). Pyroelectric tweezers for handling liquid unit volumes. Adv. Intell. Syst. ***2***(10): 2000044. https://doi.org/10.1002/aisy.202000044.
37. Gao, K., Zhang, X., Zan, Z., et al. (2019). Visible-light-assisted condensation of ultrasonically atomized water vapor on $LiNbO_3$:Fe crystals. Opt. Express ***27***(26): 37680–37694. https://doi.org/10.1364/OE.27.037680.
38. Fan, B., Li, F., Chen, L., et al. (2017). Photovoltaic manipulation of water microdroplets on a hydrophobic $LiNbO_3$ substrate. Phys. Rev. Appl. ***7***(6): 064010. https://doi.org/10.1103/PhysRevApplied.7.064010.
39. Berthier, J. (2012). Micro-drops and Digital Microfluidics (Elsevier Science).
40. Esseling, M., Zaltron, A., Horn, W., et al. (2015). Optofluidic droplet router. Laser Photon. Rev. ***9***(1): 98–104. https://doi.org/10.1002/lpor.201400133.
41. Wang, X., Bai, H., Li, Z., et al. (2023). Designing a slippery/superaerophobic hierarchical open channel for reliable and versatile underwater gas delivery. Mater. Horiz. ***10***(9): 3351–3359. https://doi.org/10.1039/D3MH00898C.
42. Bai, H., Wang, X., Li, Z., et al. (2023). Improved liquid collection on a dual-asymmetric superhydrophilic origami. Adv. Mater. ***35***(17): 2211596. https://doi.org/10.1002/adma.202211596.
43. Lin, L., Peng, X., and Zheng, Y. (2017). Reconfigurable opto-thermoelectric printing of colloidal particles. Chem. Commun. ***53***(53): 7357–7360. https://doi.org/10.1039/C7CC03530F.
44. Ashkin, A., Dziedzic, J.M., and Yamane, T. (1987). Optical trapping and manipulation of single cells using infrared laser beams. Nature ***330***(6150): 769–771. https://doi.org/10.1038/330769a0.
45. Li, Y., and Hu, Y. (2013). Localized surface plasmon-enhanced propulsion of gold nanospheres. Appl. Phys. Lett. ***102***(13): 133103. https://doi.org/10.1063/1.4799346.
46. Puerto, A., Méndez, A., Arizmendi, L., et al. (2020). Optoelectronic manipulation, trapping, splitting, and merging of water droplets and aqueous biodroplets based on the bulk photovoltaic effect. Phys. Rev. Appl. ***14***(2): 024046. https://doi.org/10.1103/PhysRevApplied.14.024046.
47. Wang, M., Gao, Z., Liu, X., et al. (2021). Towards biochemical microreactor: Nonlocal photovoltaic actuation of aqueous microdroplets in oil-infused PDMS channels based on $LiNbO_3$: Fe crystal. Sensor. Actuator. B Chem. ***349***: 130819. https://doi.org/10.1016/j.snb.2021.130819.
48. Li, J., Liu, Y., Lin, L., et al. (2019). Optical nanomanipulation on solid substrates via optothermally-gated photon nudging. Nat. Commun. ***10***(1): 5672. https://doi.org/10.1038/s41467-019-13676-3.
49. Peng, X., Chen, Z., Kollipara, P.S., et al. (2020). Opto-thermoelectric microswimmers. Light Sci. Appl. ***9***(1): 141. https://doi.org/10.1038/s41377-020-00378-5.
50. Lin, L., Kollipara, P.S., Kotnala, A., et al. (2020). Opto-thermoelectric pulling of light-absorbing particles. Light Sci. Appl. ***9***(1): 34. https://doi.org/10.1038/s41377-020-0271-6.
51. Ferraro, P., Grilli, S., Miccio, L., et al. (2008). Wettability patterning of lithium niobate substrate by modulating pyroelectric effect to form microarray of sessile droplets. Appl. Phys. Lett. ***92***(21): 213107. https://doi.org/10.1063/1.2936851.
52. Grilli, S., and Ferraro, P. (2008). Dielectrophoretic trapping of suspended particles by selective pyroelectric effect in lithium niobate crystals. Appl. Phys. Lett. ***92***(23): 232902. https://doi.org/10.1063/1.2943319.
53. Ferraro, P., Coppola, S., Grilli, S., et al. (2010). Dispensing nano-pico droplets and liquid patterning by pyroelectrodynamic shooting. Nat. Nanotechnol. ***5***(6): 429–435. https://doi.org/10.1038/nnano.2010.82.
54. Tang, X., and Wang, L. (2018). Loss-free photo-manipulation of droplets by pyroelectro-trapping on superhydrophobic surfaces. ACS Nano ***12***(9): 8994–9004. https://doi.org/10.1021/acsnano.8b02470.
55. Li, W., Tang, X., and Wang, L. (2020). Photopyroelectric microfluidics. Sci. Adv. ***6***(38): eabc1693. https://doi.org/10.1126/sciadv.abc1693.
56. Liu, M., Hua, J., and Du, X. (2024). Smart materials for light control of droplets. Nanoscale ***16***(18): 8820–8827. https://doi.org/10.1039/D3NR05593K.
57. Jin, Y., Wu, C., Sun, P., et al. (2022). Electrification of water: From basics to applications. Droplet ***1***(2): 92–109. https://doi.org/10.1002/dro2.22.
58. Liu, C., Wang, F., and Du, X. (2024). Self-powered electrostatic tweezer for adaptive object manipulation. Device ***2***(10): 100465. https://doi.org/10.1016/j.device.2024.100465.
59. Leng, X., Sun, L., Long, L., et al. (2022). Bioinspired superwetting materials for water manipulation. Droplet ***1***(2): 139–169. https://doi.org/10.1002/dro2.29.
60. Han, X., Cai, C., Deng, W., et al. (2024). Landscape of human organoids: Ideal model in clinics and research. Innovation ***5***(3): 100620. https://doi.org/10.1016/j.xinn.2024.100620.
61. Peng, M., Zhao, Q., Chai, A., et al. (2024). A ferroelectric living interface for fine-tuned exosome secretion toward physiology-mimetic neurovascular remodeling. Matter ***2025***(8): 1–14. https://doi.org/10.1016/j.matt.2024.10.019.
62. Zhou, Y., Li, J., Tan, Q., et al. (2023). Soft electronics go for three-dimensional health monitoring in deep tissue. Innov. Mater. ***1***(2): 100022. https://doi.org/10.59717/j.xinn-mater.2023.100022.
63. Zhu, X., Wang, F., Zhao, Q., et al. (2024). Adaptive interfacial materials and implants for visual restoration. Adv. Funct. Mater. ***34***(32): 2314575. https://doi.org/10.1002/adfm.202314575.

ACKNOWLEDGMENTS

The authors acknowledge the financial support provided by the National Natural Science Foundation of China (52261160380, 52022102), Shenzhen Medical Research Fund (B230245), National Key R&D Program of China (2017YFA0701303), the Youth Innovation Promotion Association of CAS (Y2023100), Guangdong Regional Joint Fund-Key Project (2021B1515120076), and the Fundamental Research Program of Shenzhen (RCJC20221008092729033, JCYJ20220818101800001).

AUTHOR CONTRIBUTIONS

X.D. came up with the concept and designed the experiments. F.W. and Z.D. carried out the experiments with assistance from W.X. and X.G. C.L. conducted the finite element analysis. X.M., Y.G., and W.Z. helped in constructing the microscopic manipulation system. X.D. supervised the study, analyzed the results, and wrote the manuscript. All authors contributed to the discussion and interpretation of the results. F.W., C.L., and Z.D. contributed equally to this work.

DECLARATION OF INTERESTS

The authors declare no competing interests.

SUPPLEMENTAL INFORMATION

It can be found online at https://doi.org/10.1016/j.xinn.2024.100742.

LEAD CONTACT WEBSITE

https://ibmd.siat.ac.cn/